Characteristics of gravity waves with short vertical wavelengths observed with radiosonde and GPS occultation during DAWEX (Darwin Area Wave Experiment)

Toshitaka Tsuda,[1] M. Venkat Ratnam,[1] Peter T. May,[2] M. Joan Alexander,[3]
Robert A. Vincent,[4] and Andrew MacKinnon[4]

Received 22 April 2004; revised 13 August 2004; accepted 27 August 2004; published 30 October 2004.

[1] We conducted radiosonde soundings during three intensive observation periods (IOP) of the Darwin Area Wave Experiment (DAWEX) campaign in October to December 2001 and measured humidity, temperature, and wind velocity up to ~30–35 km every 3 hours for 40 times at three sites in each IOP. We analyzed height profiles of kinetic (E_k) and potential (E_p) energy per unit mass caused by gravity waves with vertical wavelengths less than 3 km. The wave energy was clearly enhanced between 15–20 km and 25–30 km, and it was considerably depressed at 20–25 km between the two height regions. This feature was seen at all the sites during the three IOPs. Different types of wave activity seem to contribute to the enhancement of E_k and E_p below 20 km and at 25–30 km. Height distribution of the wave energy at 20–30 km seems to correlate with the structure of the mean zonal wind shear. We also analyzed a latitude-height section of E_p in October to December 2001 using GPS occultation data with the CHAMP satellite collected around the DAWEX sites (80–180°E and 30°N to 30°S). Compared with the latitude distribution of E_p with GPS, the DAWEX results were slightly smaller and larger at 20–25 km and 25–30 km, respectively. The longitude variation of E_p is also analyzed from the GPS data at 10–15°S, which generally agreed well with the DAWEX results at both 20–25 km and 25–30 km. *INDEX TERMS:* 3384 Meteorology and Atmospheric Dynamics: Waves and tides; 3334 Meteorology and Atmospheric Dynamics: Middle atmosphere dynamics (0341, 0342); 3314 Meteorology and Atmospheric Dynamics: Convective processes; 3374 Meteorology and Atmospheric Dynamics: Tropical meteorology; 3360 Meteorology and Atmospheric Dynamics: Remote sensing; *KEYWORDS:* gravity wave, radiosonde, GPS occultation

Citation: Tsuda, T., M. V. Ratnam, P. T. May, M. J. Alexander, R. A. Vincent, and A. MacKinnon (2004), Characteristics of gravity waves with short vertical wavelengths observed with radiosonde and GPS occultation during DAWEX (Darwin Area Wave Experiment), *J. Geophys. Res.*, *109*, D20S03, doi:10.1029/2004JD004946.

1. Introduction

[2] An intense thunderstorm known as Hector appears over the Tiwi Islands (Bathurst and Melville Islands) in the Northern Territory, Australia during the buildup to the Australian monsoon. Hector is normally associated with very strong thunderstorms, whose cloud top sometimes reaches 20 km, penetrating into the lower stratosphere. An intensive campaign to study Hector, named the Maritime Continent Thunderstorm Experiment (MCTEX), was conducted from 11 November to 8 December 1995 in order to study characteristics of island-initiated mesoscale convective system [*Keenan et al.*, 2000]. Modeling of gravity wave generation by Hector was studied using radiosonde data from MCTEX [e.g., *Lane and Reeder*, 2001].

[3] The Darwin Area Wave Experiment (DAWEX) was conducted from October to December 2001 to observe characteristics of atmospheric gravity waves excited by Hector as one of the international observation campaigns of Stratospheric Processes and Role in Climate (SPARC). A number of ground-based measurements were coordinated in DAWEX, such as radiosondes, dual-polarized C-band radar, VHF wind profilers, a medium frequency (MF) radar, and CCD airglow imagers, aimed at describing wave phenomena in a wide height range covering the boundary layer, troposphere, middle atmosphere, and lower thermosphere [*Hamilton et al.*, 2004].

[4] Through collaboration between Kyoto University, the Australian Bureau of Meteorology (BOM), Monash University, and the University of Adelaide, we carried out three campaigns of intensive radiosonde soundings with duration of 120 hours at three observation sites around

[1] Research Institute for Sustainable Humanosphere (RISH), Kyoto University, Uji, Kyoto, Japan.

[2] Bureau of Meteorological Research Center (BMRC), Melbourne, Victoria, Australia.

[3] Colorado Research Associates (CoRA), Division of Northwest Research Associates, Boulder, Colorado, USA.

[4] Department of Physics and Mathematical Physics, University of Adelaide, Adelaide, South Australia, Australia.

Copyright 2004 by the American Geophysical Union.
0148-0227/04/2004JD004946$09.00

Darwin. The intensive observation periods (IOP) were from 13–18 October (IOP1), 15–20 November (IOP2), and 11–16 December (IOP3) 2001, where an IOP was allocated just before a new moon so as to collaborate with CCD imager observations. This paper is concerned with analysis of atmospheric gravity waves by using the results from these radiosonde campaigns during DAWEX. We also employ temperature profiles observed using the GPS occultation technique with the German CHAMP (Challenging Minisatellite Payload) satellite [*Reigber et al.*, 2000].

2. Experimental Setup

[5] We selected three sites for the radiosonde soundings. The first launch site is located at Pirlangimpi (Garden Point) on Melville Island (11.4°S, 130.3°E) where Hector is expected to occur. Other two sites are the weather station of BOM at the Darwin airport (12.4°S, 130.9°E) and the Katherine civilian airport (14.5°S, 132.5°E) (a location map is shown in the work of *Hamilton et al.* [2004]). The three sites are nearly aligned toward south-southeast from Garden Point, and the distance from Garden Point to Darwin and Katherine is ~130 km and 400 km, respectively. Note that the inertial period at the three sites are ~61 hours, 56 hours, and 48 hours (from north to south), respectively, and that the entire duration of each IOP was longer than the inertial period. We continued the balloon sounding for 120 hours in each IOP in order to define the background conditions.

[6] During each IOP of DAWEX (13–18 October, 15–20 November, and 11–16 December) we started launching balloons at 1445 LT (0515 UT) on the first day of IOP and continued the soundings every 3 hours for 40 times. The balloon release timing was selected to synchronize with the twice-daily routine soundings by BOM at Darwin at 0845 LT (2315 UT) and 2045 LT (1115 UT). Thus we tried to obtain a total of 360 profiles of temperature, humidity, and wind velocity.

[7] We employed a radiosonde balloon sounding system provided by Väisälä (radiosonde type RS80) with an automatic signal processor (DigiCORA; type MW15). The horizontal location of the radiosonde was measured by means of radar tracking at Darwin and the GPS navigation at Garden Point and Katherine, respectively; then the horizontal wind velocity is calculated from time derivative of the horizontal displacement of the balloon. In order to compare the accuracy of the wind velocity determinations between the radar tracking and GPS, we launched a GPS radiosonde (RS80-15G) together with a radar reflector on 28 November 2001 from the Darwin site. Wind velocity was determined with the radar tracking every 2 s; then the results were averaged for 10 s, giving approximately 50 m height resolution. GPS data were also sampled every 2 s and interpolated to give 100 m resolution. Variance for the wind velocity difference between these simultaneous determinations was ~0.14 (m/s)^2 at 1–17 km altitude, which corresponds to the standard deviation of ~0.38 m/s. We used the profiles with a height resolution of 100 m in this paper.

[8] We employed 800 g balloons instead of the 350 g balloon used for a routine sounding at BOM, aiming to obtain profiles well into the stratosphere, up to ~30 km. Table 1 summarizes the maximum height of the balloon soundings during each IOP in October, November, and December. On average, most of balloons (97%) reached the tropopause at ~16 km, and 78% and 63% ascended up to 25 and 30 km, respectively.

[9] Because the tropical tropopause could become very cold, balloon burst (BB) sometimes occurred around the tropopause height (mostly just above the tropopause). This cooling effect is reduced during daytime due to solar radiation. A normal balloon (TA-800 by Totex Co.) is sometimes unable to reach the stratosphere. Therefore an improved balloon (TX-800), having a better performance at cold temperature, was employed at night. However, there is still a statistical difference in the BB height between day and night. Mean BB height is shown in Table 2 separately for the day and night launches. In October (IOP1) the mean BB height was nearly the same between day and night, though more BB occurred around the tropopause (between 14 and 22 km) at night. However, during the IOP2 and IOP3 the mean BB height was quite different between day and night. Although we do not know the exact reason, higher humidity in the troposphere in IOP2 and IOP3 compared with IOP1 seemed to correlate with the difference in the BB height. At Garden Point and Katherine we tried with kerosene-coated balloon in the later half of IOP3. We washed the balloon surface with kerosene for a few minutes and dried for 20–30 min before inflating it with helium. The BB height increased by ~9 km with this treatment, as shown in Table 2.

[10] Figure 1 shows height profiles of the observed eastward and northward wind velocity at Darwin during the IOP1 in October, where the successive profiles are shifted every 10 m/s, while all results are superimposed in the right of each panel. Figure 1 exhibits various wave activities with different time and vertical scales. In particular, above ~15 km there existed shorter period waves with downward phase propagating at a vertical scale of 2–3 km. It is noteworthy that the wind velocity fluctuations caused by the wave activity was small between 20 and 25 km and enhanced again above ~25 km. In the following sections we analyze the characteristics of these atmospheric waves according to the wave periods and typical vertical scales.

3. Background Conditions

[11] Here, we briefly review the background atmospheric conditions during the three IOPs. Figure 2 shows the mean profiles of the temperature, humidity, eastward and northward wind velocity, and Brunt-Väisälä frequency squared (N^2) in October, November, and December 2001. We averaged all of available radiosonde profiles at each site in each IOP; then we removed small vertical scale perturbations by applying a low-pass filter with a cutoff at 2 km and 1 km for the wind velocity and temperature profiles, respectively. The filter did not modify the overall structure of the background winds and temperature, even near the tropopause. At the lowest 1–2 km layer, we used the simple mean as the background value in order to avoid artificial modification by the edge effects of the filter.

[12] The three IOPs sampled quite different weather regimes. This is indicated by the systematic differences between the mean profiles form each IOP in Figure 2. IOP1 in October was at the beginning of the buildup phase of the wet season. At this time, deep convective storms were

Table 1. Statistics of the Balloon Burst Height During the Three IOPs of DAWEX

	Total	Below 16 km	Above 20 km	Above 25 km	Above 30 km
			October		
Garden Point	38	2	32	28	23
Darwin	38	0	35	33	27
Katherine	40	2	35	30	25
Total	116	4	102	91	75
		3%	88%	78%	65%
			November		
Garden Point	39	1	34	32	27
Darwin	39	0	29	29	28
Katherine	40	3	27	26	25
Total	118	4	90	87	80
		3%	76%	74%	68%
			December		
Garden Point	39	1	33	30	19
Darwin	36	0	32	31	31
Katherine	40	1	33	33	16
Total	115	2	98	94	66
		2%	85%	82%	57%
Total	349	10	290	272	221
		3%	83%	78%	63%

forming for the first time in the season. The tropospheric winds were westward at Garden Point and Darwin as expected in October. There was a shallow layer of eastward winds in the lowest few hundred meters associated with the heat trough to the south. On the other hand, at Katherine the zonal winds were eastward in the entire troposphere with a broad peak at 10–12 km with the maximum amplitudes of ~6 m/s.

[13] Although the mean meridional winds were generally weak in the entire height range, some structures are recognized in the troposphere. Northward winds with amplitudes of less than 3 m/s appeared below ~10 km in October. The surface wind was weakly southward at Garden Point and Darwin, and it was northward at Katherine.

[14] Temperature profiles were nearly the same between the three sites, except in the boundary layer. The cold point tropopause was located at 16.8 km, and the corresponding temperature was ~−82°C. The mean N^2 value was ~1.0–1.5 × 10^{-4} (rad/s)^2 below ~14 km, gradually increased through 15–19 km, and became fairly constant at ~6.0 × 10^{-4} (rad/s)^2 in the stratosphere.

[15] By IOP2 in November, the frequency and intensity of the convective activity in the region had increased markedly [*Hamilton et al.*, 2004]. As the monsoon trough had developed to the north, the westward winds had increased in strength and depth, i.e., peak tropospheric amplitude of ~10 m/s at around 3–4 km, having a moderate wind shear above and below. This buildup of activity was associated with a slight moistening of the lower levels, but the cold point tropopause was higher than in IOP1 by 0.3 km and significantly colder (−84.3°C). There was an extremely strong diurnal variation in convective activity at this time with very intense storms in the afternoon and some evening squall lines crossing the Darwin area in the early evening [*Hamilton et al.*, 2004]. The northward wind velocity increased to 4 m/s at 4–5 km and changed the direction toward south at 10–20 km.

[16] By IOP3 in December, the first active phase of the Australian monsoon was underway. The monsoon trough was south of Darwin and there were deep (~8 km) eastward winds observed in the soundings from Darwin and Garden Point (Pirlangimpi). This is the classic signature associated with the monsoon onset [e.g., *Holland*, 1986; *Drosdowsky*, 1996]. There were mean low-level eastward winds observed at Katherine, but these were much weaker and shallower. This is because the monsoon trough axis was almost over this site. The eastward winds were associated with a much deeper and moister humidity profile.

[17] In the lower troposphere in IOP3 the meridional wind was northward, similar to that in November, though

Table 2. Comparison of Balloon Burst (BB) Height Between Day and Night

IOP	Number of Daytime Launches	Mean BB Height During Daytime, km	Number of BB Around Tropopause	Number of Night Launches	Mean BB Height at Nighttime, km	Number of BB Around Tropopause	Difference of the Mean BB Height, km
Oct	58	30.6	3	59	29.7	10	0.9
Nov	59	31.8	4	60	27.2	25	4.5
Dec	60	32.6	1	58	26.0	16	6.7
Dec (without coating)	–	–	–	13	19.4	–	–
Dec (kerosene coating)	–	–	–	25	28.6	–	–

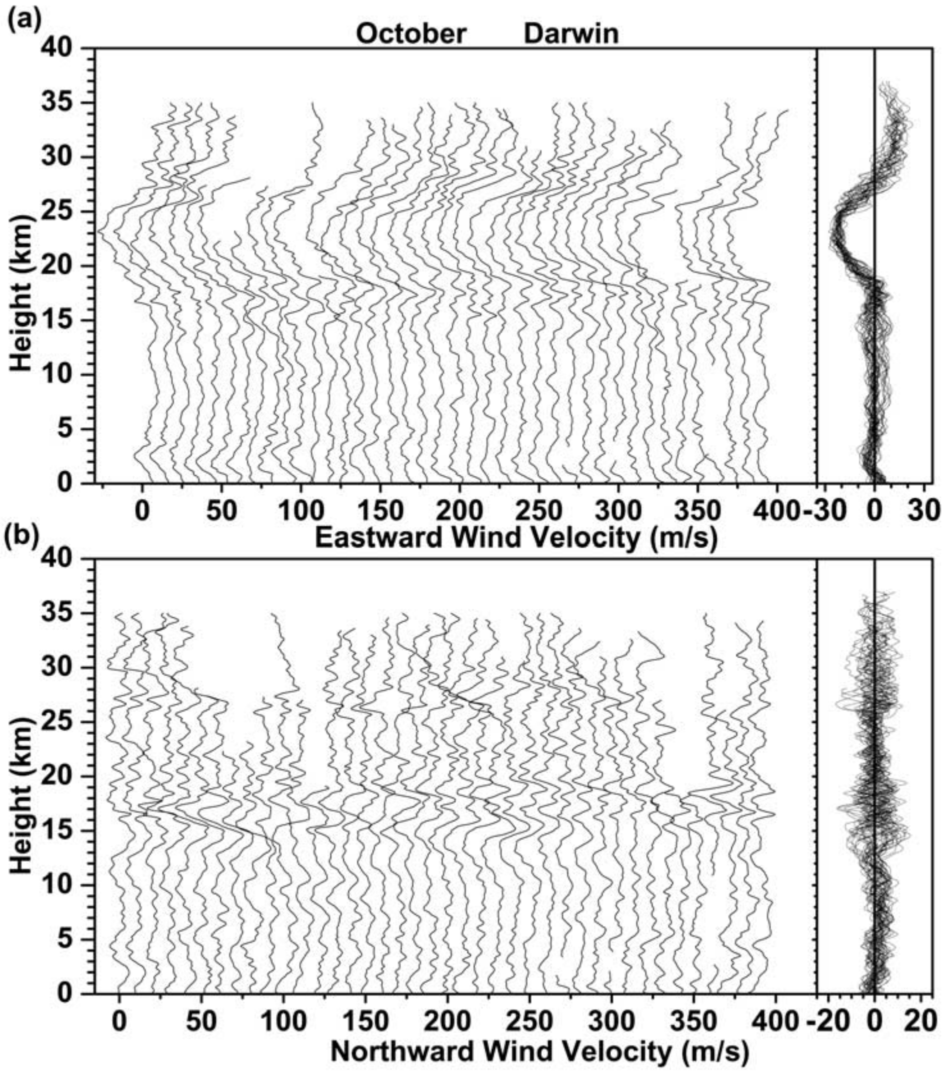

Figure 1. Profiles of (a) eastward and (b) northward wind velocity observed with three hourly radiosondes at Darwin during IOP1 (13–18 October 2001). In the left panel, individual profiles are shifted every 10 m/s, according to the launch timings (every 3 hours), while all results are superimposed in the right panel.

the peak amplitudes appeared at higher altitude. However, it became very weak without changing the direction above ~10 km. The tropopause height also decreased to 16.9 km, a similar altitude as IOP1, but on average was almost as cold as IOP2 (−83.6°C). The diurnal cycle of convection was very weak during this last IOP and the characteristics of the convection were somewhat different [*Hamilton et al.*, 2004]. The reflectivity in the convective towers decreased very rapidly above the freezing level compared with the buildup storms. This is typical of oceanic convection that is observed in the monsoon and is associated with much weaker vertical motions within the storms [e.g., *Keenan and Carbone*, 1992; *Lucas et al.*, 1994; *May and Rajopadhyaya*, 1999]. However, this does not mean that there was less rain in the monsoon convection. In fact the maximum rain rates are quite similar and the area averaged rainfall totals were larger based on radar estimates of the rainfall.

[18] Relative humidity in October ranged from 50 to 70% below ~5 km and decreased rapidly with height. The upper troposphere was fairly dry in October, but the relative humidity there increased to ~30% in November. On the other hand, the humidity in the entire troposphere considerably increased in December.

[19] There were also substantial differences between the three sounding sites. The observations at Katherine were systematically warmer and drier than those at the other sites in the lower levels. This is a reflection of it being an inland site, whereas the other sites were coastal areas. However, there were intense storms in the Katherine area as well as the coastal regions, particularly during IOP3 where there was more intense activity inland than on the coast on several days.

[20] The DAWEX IOPs coincided with the end of the easterly phase of quasi-biennial oscillation (QBO). In the stratosphere the zonal wind velocity was westward (easterly) at ~18–28 km with the maximum amplitudes of

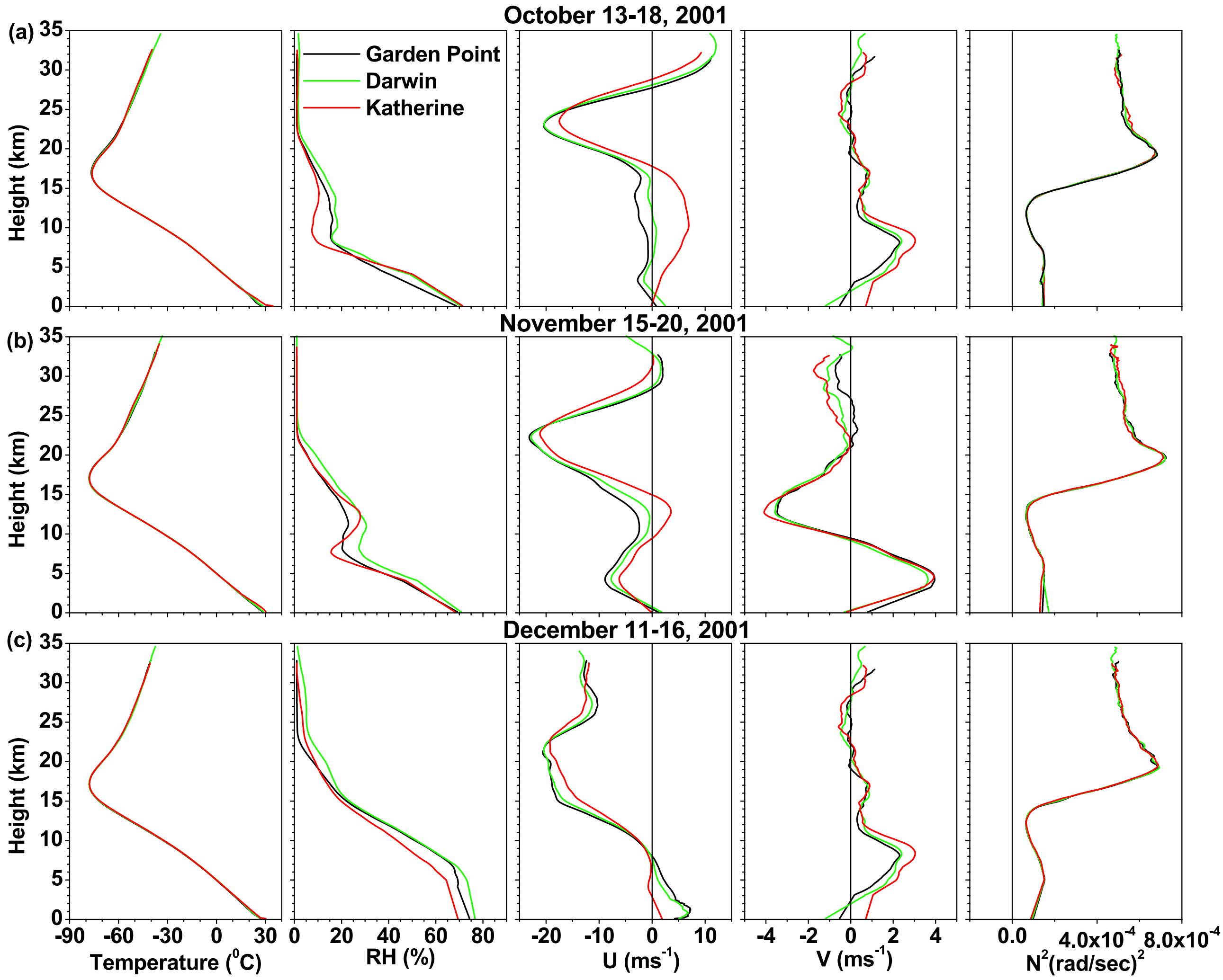

Figure 2. Mean profiles of temperature (T), relative humidity, eastward (u) and northward (v) wind velocity, and Brunt-Väisälä frequency squared (N^2) observed with radiosondes during (a) IOP1 (October), (b) IOP2 (November), and (c) IOP3 (December), respectively. Black, green, and red lines correspond to the results at Garden Point, Darwin, and Katherine, respectively. After taking an arithmetic average at each height, a boxcar smoothing over 2 km is applied for wind velocity and humidity, while a 1 km smoothing is adopted for temperature.

~20 m/s. The westward peak appeared at around 23 km in October and descended slightly to 22.5 and 22 km in November and December, respectively. The meridional wind velocity was nearly zero above ~20 km in the stratosphere.

[21] It is noteworthy that in IOP3 (December) the mean zonal wind structure at ~10–20 km appeared different from that in IOP1 and IOP2; that is, the westward wind velocity did not become weaker below 20 km, but it was as large as 15–20 m/s at 13–20 km and then it gradually decreased and reversed the direction below ~8 km. Figure 3 shows the zonal and meridional wind velocity profiles during IOP3, with the same format as Figure 1. We can see long-period wind oscillations between 13 and 20 km, whose dominant periodicity was identified as about (84 hours) 3.5 days (we discuss this phenomenon in more detail in the next section). Therefore the average wind velocity for IOP3 in Figure 2 may not represent the actual mean state caused by QBO, but it is affected by the long-period wind oscillation with the periods comparable to the campaign duration.

4. Large-Scale Oscillations Near the Tropopause

[22] Long-period wind oscillations can be seen at 12–18 km in Figures 1 and 3, though small vertical scale perturbations are also overlapped in the same height range. Spectral analysis on time series during IOP1 in October at each height indicates a dominant period of the wind oscillations as ~84 hours and 39 hours near the tropopause. In particular, the 84-hour (3.5 day) component showed a very coherent structure between the three sites. This phenomenon was also clearly detected during IOP3 (December), although it was not so evident in IOP2 (November).

[23] By applying a low-pass filter with a cutoff at 3 km, we extracted the large-scale wind components and found that the time-height structure, especially for the

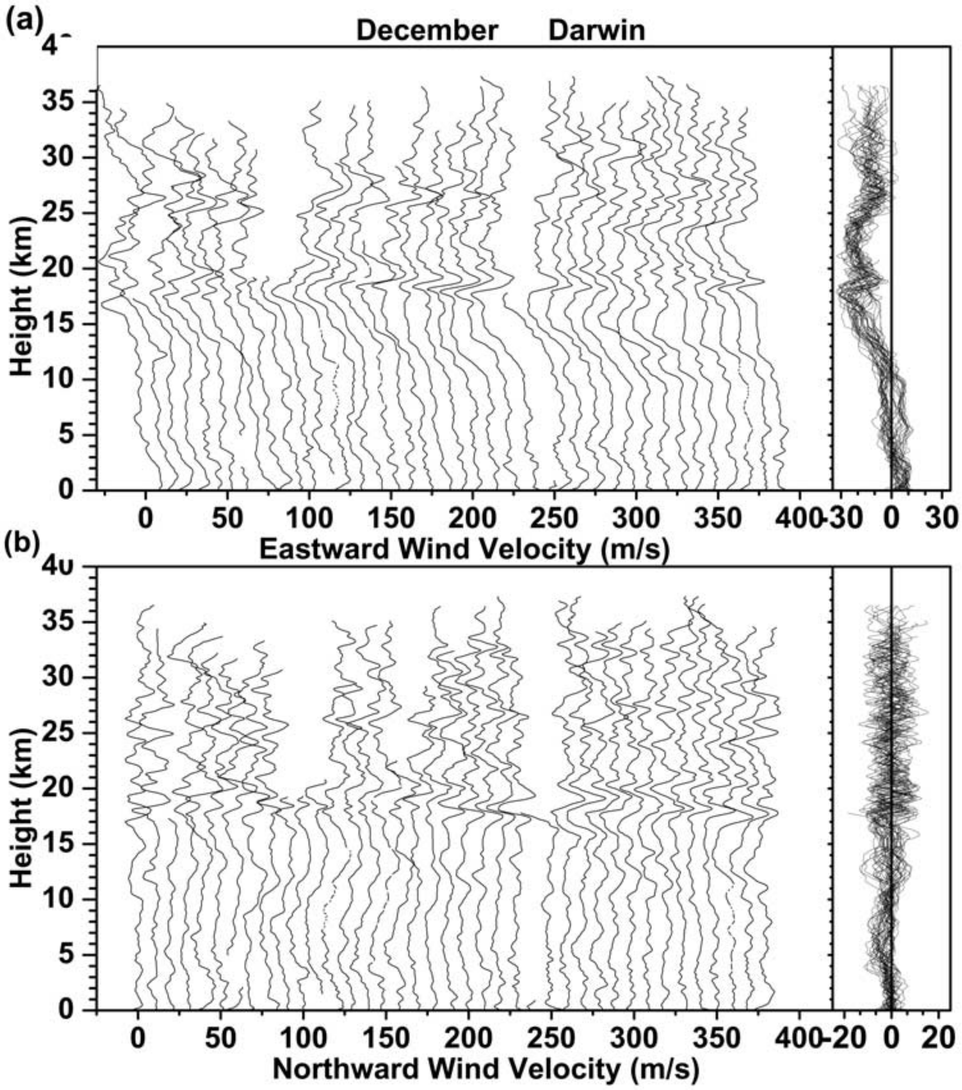

Figure 3. Same as Figure 1 except for the results during IOP3 (11–16 December 2001).

meridional winds, did not vary much between the three sites, suggesting that this long-period oscillation has a characteristic horizontal scale much larger than the extent of the three sites. Because the duration of IOPs was comparable to the wave period, we employed a periodgram analysis; that is, assuming the wave period as 84 hours, we fitted a sinusoidal curve to the temperature and wind velocity fluctuations at each height and estimated the amplitudes and relative phase. Figure 4 shows the profiles of the amplitudes and relative phases of the 84-hour oscillation during IOP3 (December). Figure 4 indicates that the 84-hour wind oscillation was enhanced between 12 and 20 km, with peak amplitudes of $\sim$4 m/s and 3 m/s for the zonal and meridional components, respectively. Associated temperature perturbations of $\sim$2 K appeared around the tropopause. Height profiles of the amplitudes and phases of the 84-hour variations in Figure 4 are nearly identical between the three sites. In particular, the downward phase progression with a vertical wavelength of $\sim$5 km was clearly recognized for both wind velocity and temperature at 15–22 km, and the phase values were almost the same between the three sites.

[24] The behavior of the 84-hour oscillations in IOP1 (October) was similar to that of IOP3, except that the enhancement was seen in a relatively narrow region between 12 and 16 km, with peak amplitudes of $\sim$6 m/s and 7 m/s for the zonal and meridional components, respectively. The temperature perturbations around the tropopause were less than 1 K. Again the height structure of amplitudes and phases was very coherent between the three sites. The phase profiles indicate a downward phase progression with a vertical wavelength of $\sim$4–6 km. During IOP2 (November), the amplitudes of the 84-hour oscillation were much smaller than in IOP1 and IOP3, and phase progression was not clear, although the height profiles were consistent between the three sites.

[25] Considering the large horizontal scale and the wave period exceeding the inertial period at the DAWEX sites, the 84-hour oscillation seems to be a planetary scale phenomenon, like an equatorial wave. The observed 84-hour oscillations seemed to be trapped near the tropo-

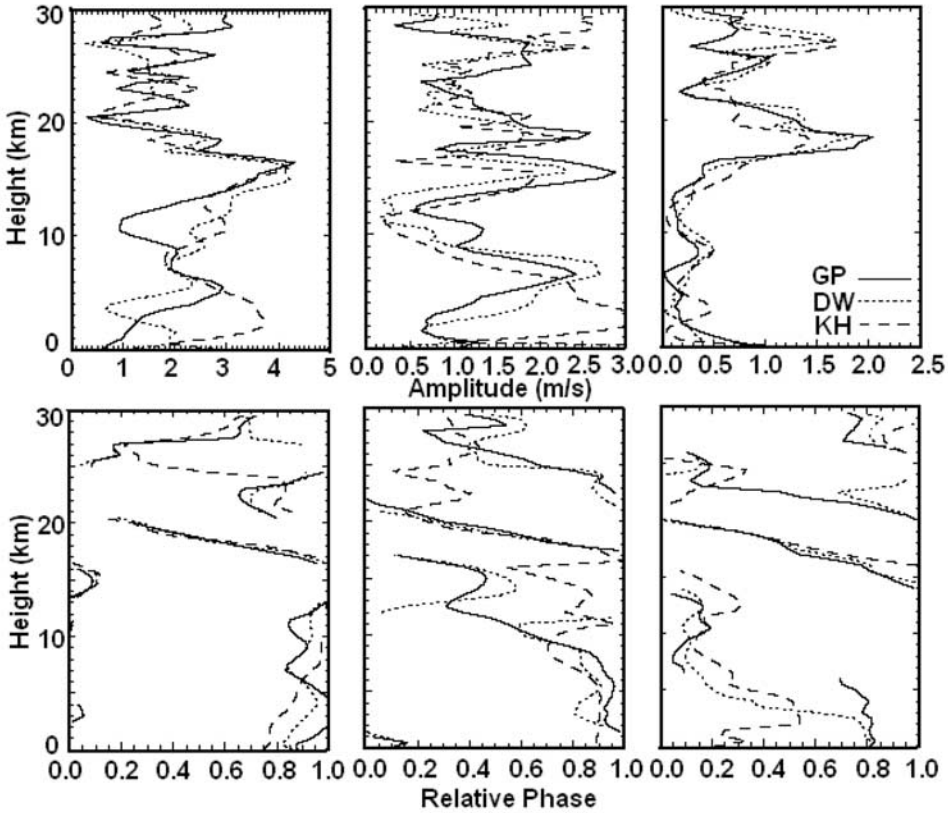

Figure 4. Height profiles of the amplitudes (top) and relative phases (bottom) of an 84-hour oscillation for the eastward and northward wind velocity and temperature (from left to right) observed with radiosondes during IOP3 of DAWEX. Solid, dotted, and broken lines correspond to the results at Garden Point, Darwin, and Katherine, respectively.

pause, giving considerable effects in the tropopause transition layer. This should be pursued in a future study.

5. Height Variations of the Kinetic (E_k) and Potential (E_p) Energy of Gravity Waves

5.1. Profiles of E_k and E_p Using Radiosonde Data

[26] From Figures 1 and 3 we recognize quite a few clear events of stratospheric gravity waves with downward phase progression having vertical wavelengths of 2–3 km. However, height distribution of the wave activity was not homogeneous. The wave amplitudes were large in the regions between 15–20 km and 25–30 km, but they were smaller between 20 and 25 km. In particular, during the IOP1 the superimposed plots of the wind velocity in Figure 1 indicate a remarkable change of the perturbation amplitudes below, within and above the 20–25 km layer.

[27] We subtracted the mean values shown in Figure 2 from individual profiles of temperature and wind velocity; then we applied a high pass filter with a cutoff at 3.1 km on the residual temperature, eastward and northward wind velocity profiles in order to remove the effects of the long-period wind oscillations. The long-period oscillations had vertical scales of ∼4–6 km, as discussed in the previous section. Time-height contour plots of the short vertical scale fluctuations at 15–20 km showed clear correlations between the three sites (figures not shown), but there existed a phase lag between the different sites; therefore they can be considered as horizontally propagating gravity waves. Nevertheless, we cannot completely rule out the possibility that a part of the perturbations with vertical scales shorter than 3 km could be contributed by a larger-scale wave like Rossby gravity wave.

[28] We estimated kinetic (E_k) and potential (E_p) energy per unit mass for gravity waves from wind velocity and temperature variance as follows:

$$E_k = \frac{1}{2}\left[\overline{u'^2} + \overline{v'^2}\right] \tag{1}$$

$$E_p = \frac{1}{2}\left(\frac{g}{N}\right)^2 \overline{\left(\frac{T'}{\overline{T_0}}\right)^2}, \tag{2}$$

where g and N are the acceleration due to gravity and the Brunt-Väisälä frequency, respectively. Prime indicates the perturbation components, and T_0 is the height-dependent mean profile shown in Figure 2. Note that u' and v' correspond to the wind velocity perturbations that are aligned or orthogonal to the wave propagation direction, respectively. However, as we cannot define the azimuthal distribution of wave propagation, we here use the perturbations of the zonal and meridional wind components for u' and v', respectively. We also neglected the effects of vertical wind velocity in equation (1).

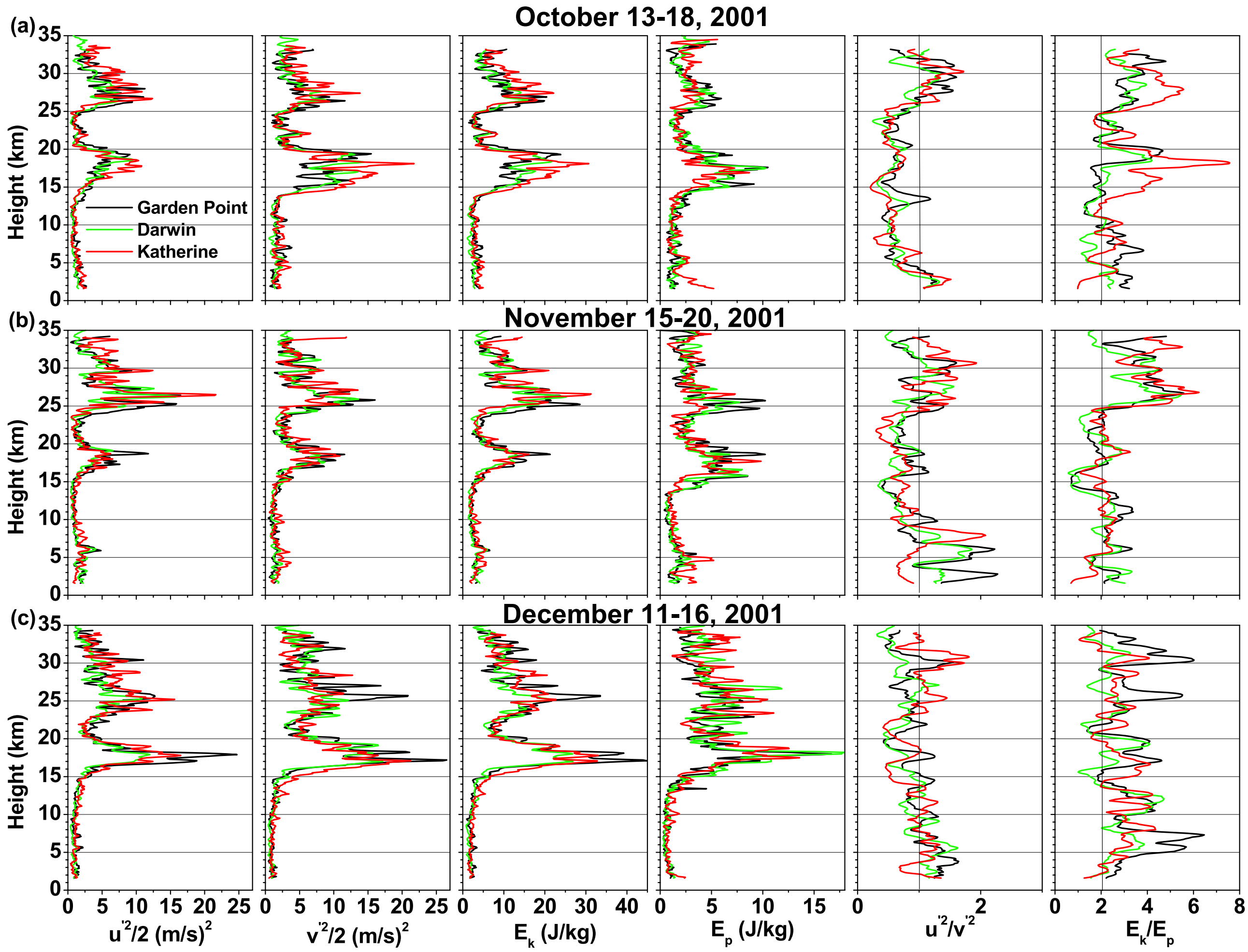

Figure 5. Mean profiles of $u'^2/2$, $v'^2/2$, E_k, E_p, u'^2/v'^2, and E_k/E_p (from left to right) for (a) IOP1, (b) IOP2, and (c) IOP3. The variance and wave energy profiles are calculated every 100 m, and the ratio is determined by smoothing for 10 height points. Black, green, and red lines correspond to the results at Garden Point, Darwin, and Katherine, respectively.

[29] We calculated E_k and E_p at each altitude (100 m height interval) from the individual high pass filtered profiles and obtained an arithmetic mean along time over all of available profiles at each site. For a monochromatic wave, E_k and E_p are normally defined by integrating the variance either along height for one wavelength or along time for one wave period. Because we averaged the variance for 40 profiles (corresponding to ~120 hours, which is longer than the inertial period) the results represent the wave energy at each height.

[30] The results are shown in Figure 5 for the three IOPs. A ratio of the wind velocity variance, u'^2/v'^2, as well as E_k/E_p is also plotted in Figure 5. The former ratio can be used as an index for the wave polarization. Considering a linear theory of gravity waves, E_k/E_p becomes a constant equal to the logarithmic spectral slope for the frequency spectrum, which was observationally reported to range from 5/3 to 2 [e.g., *VanZandat*, 1985].

[31] Table 3 summarizes the analyzed results from the three IOPs. The wave energy values are comparable to the results observed with routine radiosonde sounding at Cocos Islands (12°S, 97°E) [*Vincent and Alexander*, 2000], which is located in a convectively active region at a similar latitude to the DAWEX sites. We also calculated the wave energy per unit volume by multiplying the atmospheric density, ρ, when averaging the variance and included them in Table 3. We found that ρE_k became larger at 25–30 km than at 25–30 km in IOP1 and IOP3. However, ρE_p always decreased along altitude.

[32] The E_k profile during IOP1 in Figure 5 is characterized by a large enhancement in two separate height regions at ~15–20 km and 25–30 km and a clear depression at 20–25 km. This feature is basically common throughout the three IOPs, and there are no significant differences between the three sites in the height distribution of E_k in Figure 5.

[33] The height structure of E_p is basically very similar to that for E_k, though the enhancement above 25 km is weaker in IOP1, and the energy decrease at 20–25 km was not so clear in IOP3. Note that the lower peak of E_p appeared near the cold point tropopause at around 17 km; therefore one may suspect that any artificial temperature perturbations could contaminate into E_p because of the effects of a filtering of the sharp gradient in the temperature structure there. However, the wind velocity variance, which is not directly related to the tropopause structure, was also consistently enhanced. Moreover, the ratio E_k/E_p did not show

Table 3. Kinetic (E_k) and Potential (E_p) Energy in Three Height Layers[a]

IOP	Height, km	$u'^2/2$, J/kg	$v'^2/2$, J/kg (ρE_k, J/m^3)	E_k, J/kg	u'^2/v'^2 (ρE_p, J/m^3)	E_p, J/kg	E_k/E_p
Oct	15–20	5.4	10.3 (2.40)	15.7	0.52 (0.87)	5.4	2.9
	20–25	1.4	2.8 (0.28)	4.2	0.50 (0.12)	1.9	2.2
	25–30	5.8	5.6 (0.31)	11.5	1.04 (0.09)	3.3	3.5
Nov	15–20	3.6	5.1 (1.27)	8.7	0.71 (0.80)	5.1	1.7
	20–25	2.3	3.2 (0.32)	5.5	0.72 (0.18)	3.1	1.8
	25–30	7.3	7.1 (0.41)	14.5	1.03 (0.10)	3.6	4.1
Dec	15–20	8.0	11.3 (2.90)	19.3	0.73 (1.06)	7.0	2.8
	20–25	4.7	6.4 (0.64)	11.1	0.73 (0.32)	5.3	2.1
	25–30	6.4	7.3 (0.39)	13.7	0.88 (0.15)	5.4	2.5

[a]Here ρE_p and ρE_k per unit volume (kg/m^3) is shown in parenthesis at the three height ranges in each IOP, where ρ is atmospheric density from radiosonde measurements.

peculiar behavior around the tropopause region. We think that the E_p profile, including the tropopause region, accurately reflect the actual distribution of gravity wave activity.

[34] The enhancement of E_k and E_p in the upper region appeared at 25–28 km during IOP1, and the peak altitude decreased to ~25–27 km in IOP2; then during IOP3 the energy enhancement distributed broadly at 23–28 km. However, the lower energy peak in the 15–20 km layer did not descend, but it stayed nearly the same altitude throughout IOP1 to IOP3.

[35] The ratio of wind velocity variance u'^2/v'^2 ranged 0.5–0.7 below ~25 km in IOP1 and IOP2, and it exceeded 1 above 25 km. The energy ratio E_k/E_p also changed abruptly at ~25 km during IOP2. These variations suggest that the wave characteristics were different below and above ~25 km. However, during IOP3 both u'^2/v'^2 and E_k/E_p profiles were not clearly separated into regions with distinct characteristics.

5.2. Correlation Between the Wave Energy and Zonal Wind Shear

[36] Comparing Figures 2 and 5, the wave energy profiles seem to correlate with the mean zonal winds. That is, the energy decrease at around 20–25 km occurred in the layer of westward winds due to QBO. Provided more waves were propagating in the zonal direction, the critical level interaction and/or Doppler shifting by QBO could explain the anisotropy. However, a ratio of the zonal wind velocity variance and the meridional one was 0.5–0.7 at 20–30 km in Table 3, which could imply that more waves propagated in the meridional direction. Hodograph analysis (not shown) of some of the dominant quasi-monochromatic waves between 20 and 25 km indicated north-south propagation, so these waves would be unaffected by the zonal wind shear.

[37] Because the background mean meridional winds were nearly zero above the tropopause, interaction of gravity waves with the meridional winds was probably not responsible for the minimum. Note that N^2 in Figure 2 was nearly constant above the tropopause, which does not explain height variations of E_k and E_p.

[38] Enhancement of E_k at around 25 km occurred in the region of large eastward wind shear above the westward peak of QBO. We calculated the zonal wind shear from height derivative of the mean zonal wind in Figure 2 and averaged it for the three sites. Figure 6 shows the mean zonal wind velocity and zonal wind shear in three IOPs compared with the mean profile of E_k and E_p. The eastward wind shear became large at 25–30 km with a peak at 27 km in IOP1, and the peak descended to 26 km in IOP2 and 24 km in IOP3. The maximum shear amplitude decreased linearly from 5.7 m/s/km in IOP1 to 4.5 m/s/km in IOP2 and 2.5 m/s/km in IOP3. The peak of E_k seemed to coincide with the peak of eastward wind shear in Figure 6. However, the amplitudes of E_k and E_p did not correlate with the shear intensity. Note that the westward wind shear with a peak at 20 km in IOP1 also descended to 18 km in IOP2 and 14 km in IOP3, but the region of large wave energy stayed in the 15–20 km altitude.

[39] The evidence presented here suggests that the two peaks in the variance profiles, one below 20 km and the other above 25 km, are due to different types of wave activity. Here, we discuss a possible mechanism that explains the height structure of the wave activity. *Alexander et al.* [2004] proposed a model on wave generation by convection in the Darwin area, which are characterized by short horizontal wavelength (40–150 km) with phase speeds peaking at 5–10 m/s propagating in the northeast direction. They reported a dramatic increase in variance for these waves above 25 km because of the combined effects of background wind shear and growth due to decreasing density.

[40] The observed peak of the wave energy above 25 km in Figure 5 is consistent with the results of *Alexander et al.* [2004]. Although their model focuses on 1 day in IOP2 (November), the resulting wave properties were strongly dependent on the background wind profile, particularly the upper tropospheric westward shear. This feature of the wind did not change dramatically through the IOP2 and was similar to the IOP1 (October). The lower variance peaks observed in the radiosonde analyses below 20 km were not reproduced in the work of *Alexander et al.* [2004]. This lower peak could be due to larger horizontal scale waves not resolved in the model by *Alexander et al.* [2004] and that may be generated by sources outside the local Darwin area.

6. Comparison of E_p Between Radiosondes and GPS Occultation

[41] We analyzed temperature variance with vertical scales smaller than ~3 km using individual temperature profiles observed by GPS occultation with the German CHAMP satellite and then estimated E_p. Figure 7 shows the distribution of GPS occultation data (a total of 776 events) during 3 months from October to December 2001,

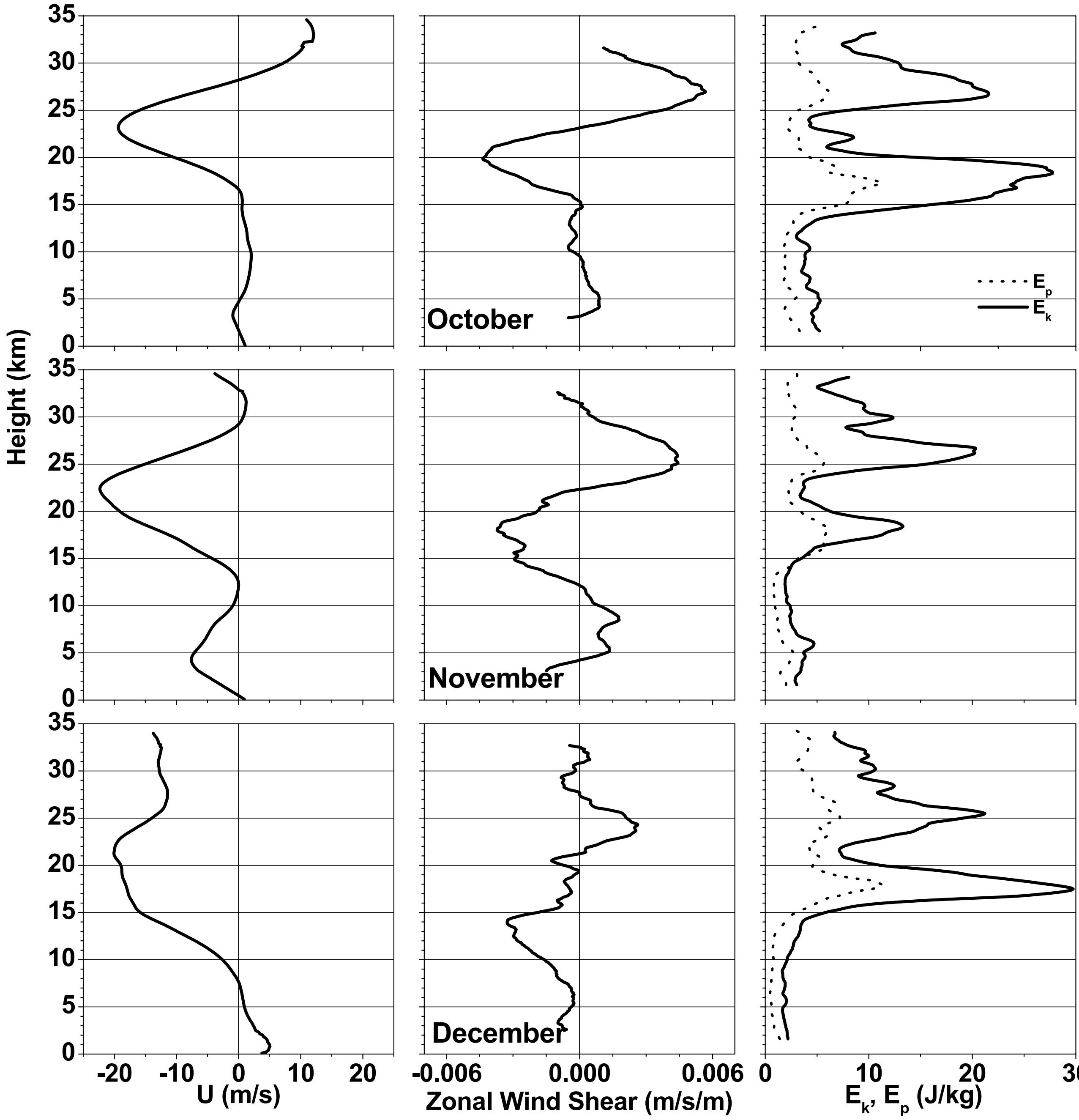

Figure 6. Profiles of the mean eastward wind velocity (left), the zonal wind shear (center), and the mean E_k (solid line) and E_p (dotted line) profiles (right) averaged for the three sites in IOP1 (top), IOP2 (middle), and IOP3 (bottom).

between 30°N to 30°S and 80° to 180°E in latitude and longitude, respectively. Figure 8 shows a latitude height section of E_p, where the E_p values are averaged along longitude in 80–180°E. Fundamental structure in Figure 8, such as enhancement of E_p in the equatorial region and decrease above ~25 km, are basically consistent with earlier studies using GPS occultation data [*Tsuda et al.*, 2000; *Tsuda and Hocke*, 2004; *Ratnam et al.*, 2004]. From intermittent CHAMP/GPS results we were unable to define the background temperature profile by taking their time average. So temperature fluctuations obtained as a residual of filtering may be affected by the large temperature gradient near the tropopause. Therefore we do not analyze E_p with GPS occultation data below 20 km in the present study.

[42] The wave energy in Figure 8 was enhanced below ~24 km, showing a symmetric distribution between the Northern and Southern Hemispheres. The top height of the large E_p layer extended to ~24 km over the equator; then it rapidly decreased to 22 km at around 7–12° in latitude and E_p became sharply smaller outside 25°. Potential energy was clearly depressed above ~25 km, and it again increased above ~30–32 km. Decrease of the equatorial peak on E_p above 25 km was reported by earlier GPS analysis [*Tsuda et*

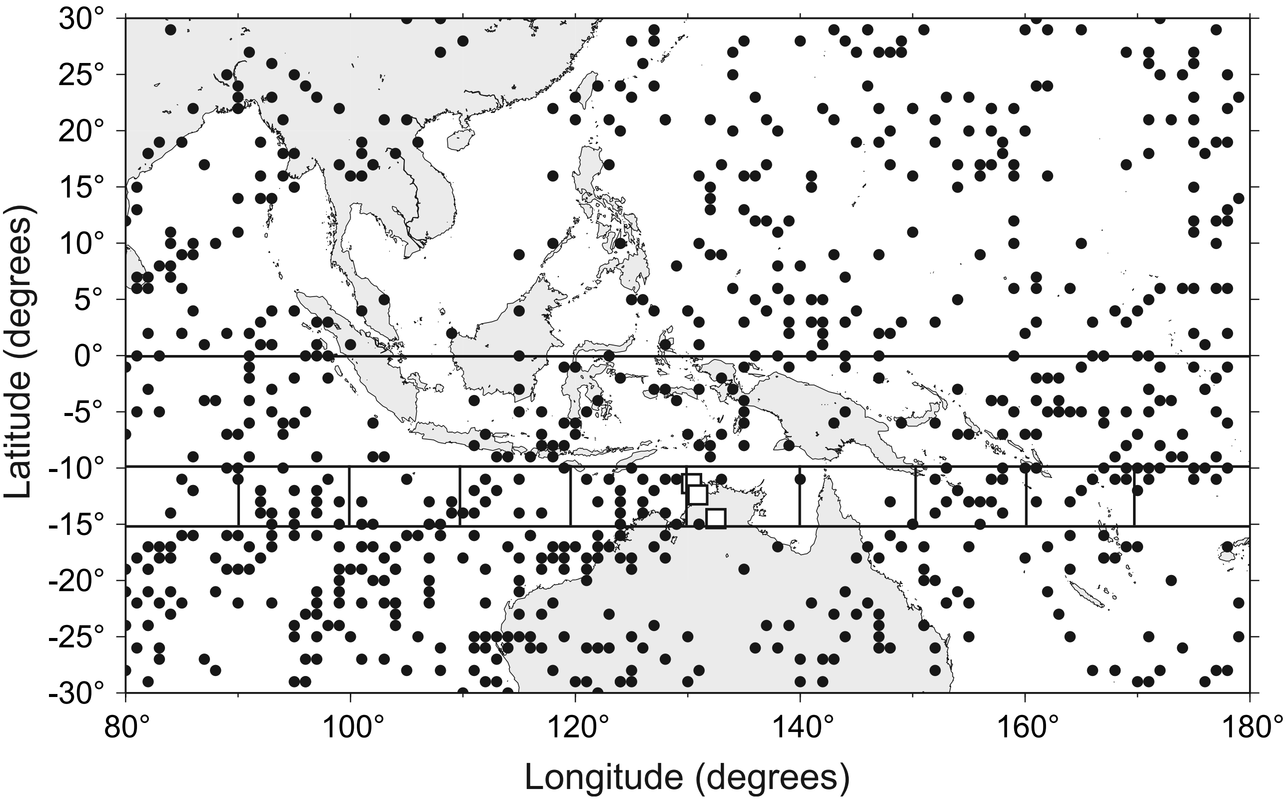

Figure 7. Distribution of the CHAMP GPS occultation data (dot) in October to December 2001. Radiosonde launch sites are also indicted by an open square.

al., 2000; *Ratnam et al.*, 2004], and it was also detected by CRISTA observations [*Preusse et al.*, 2000].

[43] In Figure 8, E_p at 10–20°N did not monotonically decrease along altitude, but it showed a minimum at 22–25 km and a second enhancement of E_p appeared above ~25 km. That is, a branch of large E_p seemed to expand from the equatorial region obliquely upward toward middle latitudes. Although the fundamental structure of the latitude-height distribution of E_p above 20 km looks similar to that in the Northern Hemisphere, the corresponding branch of E_p was not clearly identified in the Southern Hemisphere in Figure 8 because of coarse resolution of the contour plot. We calculated a mean profile of E_p averaging the GPS results in Figure 8 in a region around the DAWEX sites, i.e., in 11–15°S and 80–180°E, and compared it in Figure 9 with the mean E_p profiles with radiosondes averaged throughout IOP1, IOP2, and IOP3. The GPS analysis clearly shows an enhancement of E_p centered at 25 km and a local minimum at ~22–23 km, which are generally consistent with the DAWEX radiosondes results, although detailed structure did not match perfectly, probably because the period and area of the observations are not exactly the same between GPS and radiosondes.

[44] Figure 10 shows a latitude distribution of E_p for perturbations with short vertical wavelengths (<3 km) averaged in a height layer of 20–25 km and 25–30 km, which is basically equivalent to a latitude section of the E_p distribution in Figure 8. The latitude variation showed a clear contrast between the two height ranges; that is, at 20–25 km, E_p was large over the equator with the maximum E_p value of ~11 J/kg, and there was a bell-shape distribution along latitude, decreasing to 2–3 J/kg at 30°. The latitude variation of E_p is generally consistent with earlier studies with radiosondes and GPS occultation [*Allen and Vincent*, 1995; *Alexander et al.*, 2002]. Though the latitude distribution at 20–25 km is basically symmetric, E_p at 15°–20° was slightly larger in the Northern Hemisphere. The latitude distribution was rather featureless at 25–30 km and does not show evident latitude dependence, though E_p at 15°–20° N was again larger by ~40% compared with that at 15°–20°S. The DAWEX results were smaller than the latitude distribution at 20–25 km in Figure 10, while they exceeded the GPS results by a factor of ~1.4 at 25–30 km.

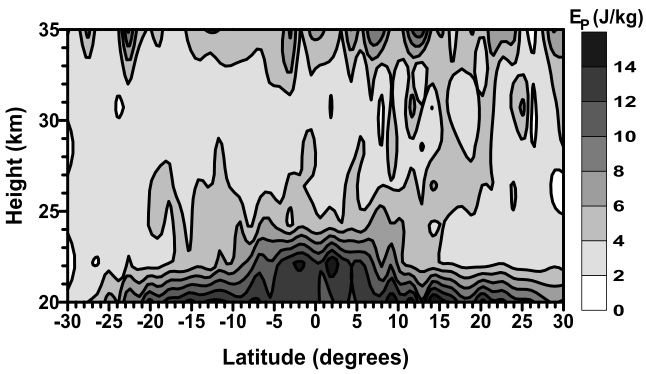

Figure 8. Latitude height section of E_p observed with CHAMP/GPS occultation in October to December 2001 in a longitude band of 80–180°E. Temperature variance is estimated by extracting perturbations with vertical scale shorter than 3 km from individual profiles.

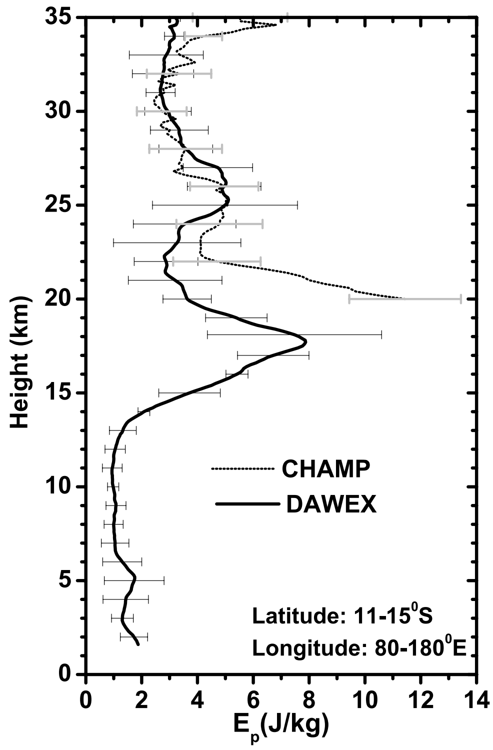

Figure 9. Mean profile of E_p analyzed by using all of CHAMP-GPS data (dashed line) observed in October to December 2001 at 11–15°S and 80–180°E, in comparison with the mean E_p profile from the DAWEX radiosondes (solid line).

[45] The discrepancy can be partially caused by the difference in the horizontal and vertical resolution between the GPS occultation and radiosondes [*Tsuda et al.*, 2000]. It is noteworthy, however, that the upper peak of E_p in Figure 9 appeared at a slightly lower altitude for GPS than the DAWEX radiosondes. By selecting the height range for averaging at 25–30 km, the DAWEX results could become larger than GPS in Figure 10a. Therefore the discrepancy in Figure 10 could also be attributed to the difference in the time interval and area for averaging the observed profiles.

[46] We show in Figure 11 longitude variation of E_p at 20–25 km and 25–30 km using GPS occultation data in 10–15°S. At 20–25 km the E_p values varied from 4.2 to 7 J/kg, with a minimum at 130–140°E. Although the DAWEX results were smaller than the zonal mean of E_p in Figure 10, it is consistent with the longitude variation of E_p. At 25–30 km the E_p values became a maximum at 120–130°E, and the DAWEX data agreed well with the longitude variation of the GPS results. *de la Torre et al.* [2004] tried to identify the longitude distribution of E_p during the DAWEX period in the tropics. However, correlation between the E_p enhancement and the distribution of convection and/or topography was not entirely clear, mainly because of sparse CHAMP data at low latitudes.

7. Concluding Remarks

[47] We successfully conducted radiosonde campaigns at three observation sites around Darwin, Northern Australia during the three IOPs of DAWEX, which coincided with the premonsoon to monsoon-onset periods. In each IOP, balloons were launched every 3 hours for 120 hours. A total of 351 profiles are obtained in the troposphere and lower stratosphere up to 30–35 km. We analyzed the background conditions of winds and temperature and then studied the behavior of atmospheric gravity waves. The main results are summarized in the following.

[48] 1. Background zonal winds were affected by QBO, showing westward winds of ~20 m/s at 20–25 km. Meridional winds were nearly zero.

[49] 2. Near the tropopause (12–18 km), long-period oscillations were enhanced for both temperature and wind velocity. In particular, an 84-hour oscillation was evident in October and December. Height structure of these oscillations was coherent between the three sites, suggesting a large horizontal scale of the wave, like an equatorial wave.

[50] 3. We estimated wave kinetic (E_k) and potential energy (E_p) from wind velocity and temperature fluctuations with vertical wavelengths shorter than ~3 km. Both E_k and E_p became large at the 15–20 km and 25–30 km height ranges, but they were clearly depressed at 20–25 km. The large wave energy at 20–30 km seemed to appear in the height region of large eastward shear of zonal winds.

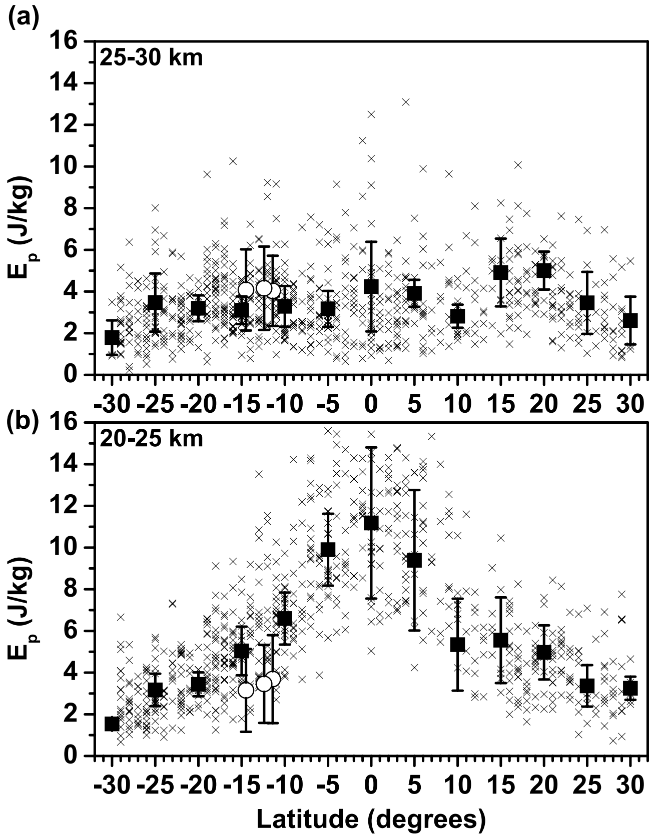

Figure 10. Latitude variation of E_p for temperature perturbations with vertical scales shorter than 3 km at (a) 25–30 km and (b) 20–25 km from individual CHAMP/GPS data (cross), and DAWEX radiosonde results are also plotted (circle). Square symbol shows the mean and the standard deviation of E_p every 5° in latitude. (The mean value at 30° corresponds to E_p averaged in the 27.5°–30° latitude.)

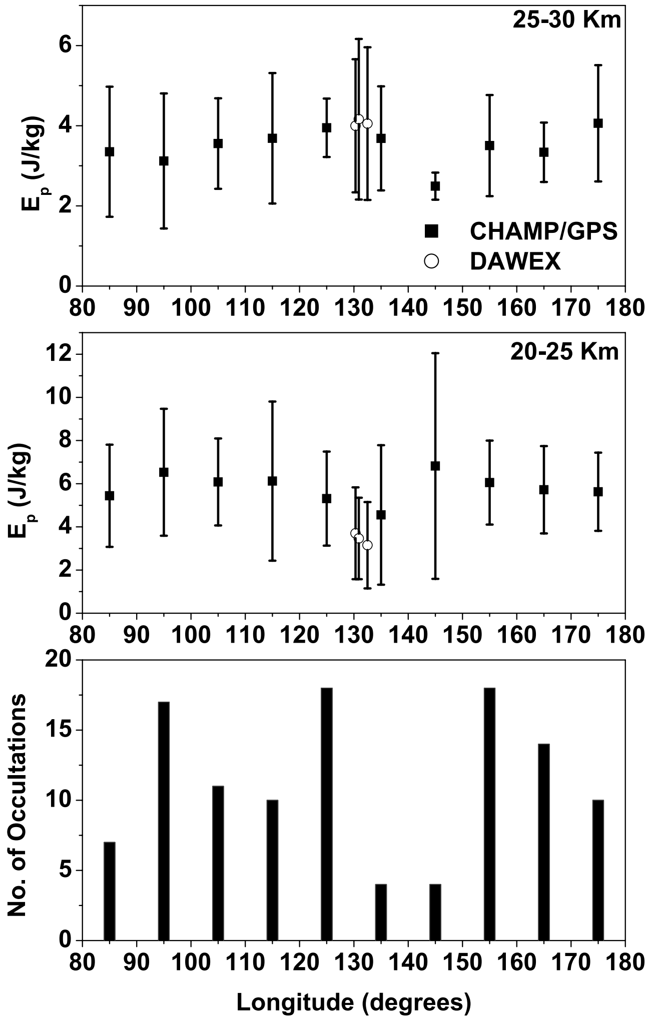

Figure 11. Longitude variation of E_p from CHAMP/GPS data at 10–15°S in each 10° longitude sector (indicated by a box in Figure 7) in the 25–30 km (top) and 20–25 km layers (middle). DAWEX radiosonde results are also plotted (open circle). Number of GPS data in each 10° longitude sector is shown in the bottom.

[51] 4. Although we identified enhancement of E_p in two separate height regions at 15–20 km and 25–30 km, the origin of gravity waves at these height ranges seems to be different. The abrupt increase of the wave energy above ~25 km is consistent with a model prediction for convective generation of gravity waves [*Alexander et al.*, 2004].

[52] 5. The latitude-height distribution of E_p was determined in the tropical Pacific and Indian Ocean (80–180°E and 30°N to 30°S) by using GPS occultation data with CHAMP in October to December 2001. Potential energy values from DAWEX were smaller/larger than the latitude distribution of the zonal mean E_p with GPS at 20–25 km and 25–30 km, respectively. Longitude distribution of E_p was determined at 10–15°S by using GPS data, which agreed well with the DAWEX results. The height structure of E_p at 20–30 km from DAWEX data is consistent with the global distribution of E_p determined with GPS occultation data.

[53] **Acknowledgments.** We greatly appreciate the extensive participation for the balloon experiments by Ross Christmas, Nigel Mules, Jim Arther, Ken Glasson, Tim Buckley, Phil Dutton, Roger Atkinson, and their colleagues at BOM in Darwin; Simon Alexander and Peter Love from the University of Adelaide; Tim Barns from NCAR; Y. Aoyama, T. Yoshihara, and T. Shimabukuro from Kyoto University; and Fiona Guest, Robert Goler, Andrew Marshal, Stewart Allen, Sylvain Manso, Ivan Mac, Justin Peters, Kirsty Fletcher, Briony MacPherson, Jin Lee, Michael Logan, Andrew Roberts, Salah Jimi, Michael Duell, and Michael Reeder from Monash University. We are grateful for continuous encouragement by Kevin Hamilton. We wish to thank GFZ Potsdam for providing CHAMP/GPS data through the ISDC data center. This study is partially supported by the grant-in-aid for scientific research 13573005 and 13136203 provided by Japan Society for Promotion of Science (JSPS).

References

Alexander, M. J., T. Tsuda, and R. A. Vincent (2002), Latitudinal variations observed in gravity waves with short vertical wavelengths, *J. Atmos. Sci.*, *59*, 1394–1404.

Alexander, M. J., P. T. May, and J. Beres (2004), Gravity waves generated by convection in the Darwin area during the Darwin Area Wave Experiment, *J. Geophys. Res.*, *109*, D20S04, doi:10.1029/2004JD004729.

Allen, S., and R. Vincent (1995), Gravity wave activity in the lower atmosphere: Seasonal and latitudinal variations, *J. Geophys. Res.*, *100*, 1327–1350.

de la Torre, A., T. Tsuda, G. A. Hajj, and J. Wickert (2004), A global distribution of the stratospheric gravity wave activity from GPS occultation profiles with SAC-C and CHAMP, *J. Meteorol. Soc. Jpn.*, *82*, 407–417.

Drosdowsky, W. (1996), Variability of the Australian summer monsoon at Darwin: 1957–1992, *J. Clim.*, *9*, 85–96.

Hamilton, K., R. A. Vincent, and P. T. May (2004), Darwin Area Wave Experiment (DAWEX) field campaign to study gravity wave generation and propagation, *J. Geophys. Res.*, *109*, D20S01, doi:10.1029/2003JD004393, in press.

Holland, G. J. (1986), Interannual variability of the Australian summer monsoon at Darwin: 1952–82, *Mon. Weather Rev.*, *114*, 594–604.

Keenan, T., and R. E. Carbone (1992), A preliminary morphology of precipitation systems in tropical northern Australia, *Q. J. R. Meteorol. Soc.*, *118*, 283–326.

Keenan, T., et al. (2000), The maritime continent thunderstorm experiment (MCTEX): Overview and some results, *Bull. Am. Meteorol. Soc.*, *81*, 2433–2455.

Lane, T. P., and M. Reeder (2001), Modeling the generation of gravity waves by a maritime continent thunderstorm, *Q. J. R. Meteorol. Soc.*, *127*, 2705–2724.

Lucas, C., E. J. Zipser, and M. A. LeMone (1994), Vertical velocity in oceanic convection off tropical Australia, *J. Atmos. Sci.*, *51*, 3183–3193.

May, P. T., and D. K. Rajopadhyaya (1999), Vertical velocity characteristics of deep convection over Darwin, Australia, *Mon. Weather Rev.*, *127*, 1056–1071.

Preusse, P., S. D. Eckermann, and D. Offermann (2000), Comparison of global distributions of zonal-mean gravity wave variance inferred from different satellite instruments, *Geophys. Res. Lett.*, *27*, 3877–3880.

Ratnam, M. V., G. Tetzlaff, and C. Jacobi (2004), Global and seasonal variations of stratospheric gravity wave activity deduced from the Challenging Minisatellite Payload (CHAMP) GPS satellite, *J. Atmos. Sci.*, *61*, 1610–1620.

Reigber, C., H. Lühr, and P. Schwintzer (2000), CHAMP mission status and perspectives, *Eos Trans. AGU*, *81*(48), Fall Meet. Suppl., F307.

Tsuda, T., and K. Hocke (2004), Application of GPS radio occultation data for studies of atmospheric waves in the middle atmosphere and ionosphere, *J. Meteorol. Soc. Jpn.*, *82*, 419–426.

Tsuda, T., M. Nishida, C. Rocken, and R. H. Ware (2000), A global morphology of gravity wave activity in the stratosphere revealed by the GPS occultation data (GPS/MET), *J. Geophys. Res.*, *105*, 7257–7273.

VanZandt, T. E. (1985), A model for gravity wave spectra observed by Doppler sounding system, *Radio Sci.*, *20*, 1323–1330.

Vincent, R. A., and M. J. Alexander (2000), Gravity waves in the tropical lower stratosphere: An observational study of seasonal and interannual variability, *J. Geophys. Res.*, *105*, 17,971–17,982.

M. J. Alexander, Colorado Research Associates (CoRA), Division of Northwest Research Associates, 3380 Mitchell Lane, Boulder, CO 80301, USA.

A. MacKinnon and R. A. Vincent, Department of Physics and Mathematical Physics, University of Adelaide, Adelaide 5005, Australia.

P. T. May, Bureau of Meteorological Research Center (BMRC), P. O. Box 1289K, Melbourne, Victoria 3001, Australia.

M. V. Ratnam and T. Tsuda, Research Institute for Sustainable Humanosphere (RISH), Kyoto University, Uji, Kyoto 611-0011, Japan. (tsuda@rish.kyoto-u.ac.jp)